Managing Interfacial Defects and Carriers by Synergistic Modulation of Functional Groups and Spatial Conformation for High-Performance Perovskite Photovoltaics Based on Vacuum Flash Method

Deyu Gao, Ru Li, Xihan Chen, Cong Chen, Chenglin Wang, Boxue Zhang, Mengjia Li, Xueni Shang, Xuemeng Yu, Shaokuan Gong, et al.

Managing Interfacial Defects and Carriers by Synergistic Modulation of Functional Groups and Spatial Conformation for High-Performance Perovskite Photovoltaics based on Vacuum Flash Method

Deyu Gao[#a,b], Ru Li[# c], Xihan Chen[d#], Cong Chen[a,b*], Chenglin Wang[b], Boxue Zhang[e], Mengjia Li[b], Xueni Shang[b], Xuemeng Yu[d], Shaokuan Gong[d], Thierry Pauporté[e], Hua Yang[f], Liming Ding[g*], Jian-Xin Tang[a,h*], and Jiangzhao Chen[c*]

[a]Macao Institute of Materials Science and Engineering (MIMSE), Faculty of Innovation Engineering, Macau University of Science and Technology, Taipa, Macau SAR 999078, Macao, China

[b]State Key Laboratory of Reliability and Intelligence of Electrical Equipment, School of Materials Science and Engineering, Hebei University of Technology, Tianjin 300401, China

[c]Key Laboratory of Optoelectronic Technology & Systems (Ministry of Education), College of Optoelectronic Engineering, Chongqing University, Chongqing 400044, China

[d]SUSTech Energy Institute for Carbon Neutrality, Department of Mechanical and Energy Engineering, Southern University of Science and Technology, Shenzhen 518055, Guangdong,China

[e]CNRS, Institut de Recherche de Chimie Paris (IRCP), UMR8247, Chimie ParisTech, PSL Research University, F-75005 Paris, France

This article has been accepted for publication and undergone full peer review but has not been through the copyediting, typesetting, pagination and proofreading process, which may lead to differences between this version and the Version of Record. Please cite this article as doi: 10.1002/adma.202301028.

[g]Institute of High Energy Physics, Chinese Academy of Sciences (CAS), Beijing 100049, China

[f]Center for Excellence in Nanoscience (CAS), Key Laboratory of Nanosystem and Hierarchical Fabrication (CAS), National Center for Nanoscience and Technology, Beijing 100190, China
[h]Collaborative Innovation Center of Suzhou Nano Science & Technology, Institute of Functional Nano & Soft Materials (FUNSOM), Soochow University, Suzhou, Jiangsu 215123, China

*Corresponding authors

E-mail: chencong@hebut.edu.cn (C.C), ding@nanoctr.cn (L.D.), jxtang@must.edu.mo (J.T), jiangzhaochen@cqu.edu.cn (J.C.)

# These authors contributed equally to this work.

Abstract

Interfacial nonradiative recombination loss is a huge barrier to advance the photovoltaic performance. Here, we propose one effective interfacial defect and carrier dynamics management strategy by synergistic modulation of functional groups and spatial conformation of ammonium salt molecules. The surface treatment with 3-ammonium propionic acid iodide (3-APAI) does not form 2D perovskite passivation layer while the propylammonium ions and 5-aminopentanoic acid hydroiodide post-treatment lead to the

formation of 2D perovskite passivation layers. Due to appropriate alkyl chain length, theoretical and experimental results manifest that -COOH and -NH_3^+ groups in 3-APAI molecules can form coordination bonding with undercoordinated Pb^{2+} and ionic bonding and hydrogen bonding with octahedron PbI_6^{4-}, respectively, which makes both groups be simultaneously firmly anchored on the surface of perovskite films. This would strengthen defect passivation effect and improve interfacial carrier transport and transfer. The synergistic effect of functional groups and spatial conformation confers 3-APAI better defect passivation effect than 2D perovskite layers. The 3-APAI modified device based on vacuum flash technology achieves an alluring peak efficiency of 24.72% (certified 23.68%), which is among highly efficient devices fabricated without antisolvents. Furthermore, the encapsulated 3-APAI-modified device degrades by less than 4% after 1400 h of continuous one sun illumination.

Keywords: Perovskite solar cells, interfacial engineering, functional groups, spatial conformation, synergistic modulation

1. Introduction

Perovskite solar cells (PSCs) have been considered as one of the most promising next-generation photovoltaic technologies on account of its superb photoelectrical properties and

solution processing property of metal halide perovskite absorbers.[1-4] Since the first report on the all-solid-state PSCs,[5] mammoth research advancements in power conversion efficiency (PCE) and long-term operational stability have been accomplished.[6-9] The single junction and tandem PSCs have demonstrated a record certified PCE of 25.7% and 32.5%, respectively.[10] Presently, most of high-efficiency PSCs were constructed based on the perovskite films prepared by antisolvents.[4, 9, 11-13] However, most commonly used antisolvents (e.g., chlorobenzene and diethyl ether) are toxic and antisolvent procedure is not beneficial for large scale production. Consequently, it is imperative develop antisolvent-free fabrication techniques to prepare high-quality perovskite films. Although vacuum flash-assisted solution process method has been reported several years ago,[14] the PCEs of the devices based on vacuum flash are far behind than those of the devices using antisolvent approach. In recent several years, interface engineering has made enormous contributions to realizing efficient and stable perovskite photovoltaics.[6, 9, 15, 16] More efforts should be focused on manipulating interface in order to minimize interfacial nonradiative recombination and thus enhance open-circuit voltage (V_{OC}) and fill factor (FF) in the following research work.

It is well known that trap-assisted nonradiative recombination has a profound impact on V_{OC} and FF.[1] The trap density at the interface and grain boundaries (GBs) was uncovered

to be much larger trap density than that within the bulk of perovskite films.[17-19] Moreover, the deep level defects are usually in the presence of interface and GBs, which would bring about grievous carrier nonradiative recombination.[20, 21] In order to passivate interfacial defects, various passivators have been exploited, mainly including Lewis acids,[22] Lewis bases,[9, 23, 24] 2D perovskites[15, 25, 26] and organic/inorganic salts[27-32]. Multifarious donor and accepter type defects could be simultaneously at interface. Nevertheless, Lewis acid and Lewis base normally only can heal negatively charged defects (e.g., cation vacancy, Pb^{2+} vacancy, and PbI_3^- antisite defects) and positively charged defects (e.g., halide vacancy and uncoordinated Pb^{2+} defects), respectively.[23, 33] Constructing 2D perovskite interface layer has been considered to be one universal route to passivate interfacial defects.[15, 25, 26, 34] However, the high exciton binding energy and poor carrier transport of 2D perovskites are not conducive to interfacial carrier transport and transfer and accordingly minimizing interfacial nonradiative recombination. Furthermore, it is still a huge challenge for 2D perovskites to achieve simultaneous passivation of anionic and cationic defects. Recently, Xing et al.[35] revealed photoinduced carrier blocking effect due to a photoinduced potential barrier reaching several hundred meV, which jeopardized short-circuit current density (J_{SC}) and FF. Consequently, 2D perovskite may not be one optimal interfacial defect passivation method.

Compared with Lewis acid, Lewis base and 2D perovskites, organic/inorganic salts could be more promising considering that they can simultaneously passivate positively and negatively charged defect.[27, 30-32, 36] In contrast to inorganic salts, organic salts could be more attractive due to their structural adjustability.[31, 37, 38] In recent two years, optimizing interfacial defect passivation effect is one of main research topics from the perspective of modulating and optimizing molecular structures of organic salts.[30, 32, 36] Yang et al.[32] adopted PRA, PRMA, and PREA organic salts to modify the surface of perovskite films and demonstrated that PREA with a properly tailored intercalation distance between layers of the inorganic framework contributed to the surface band edges and influenced the carrier dynamics, which augmented hole mobilities, improved device efficiency and stability. This indicates that the spatial conformation of organic salts plays a pivotal role in passivating interfacial defects and reconfiguring the band-edge states. In addition, increasing the number of active sites in passivators can effectively strengthen chemical interaction strength between modifiers and perovskites by multidentate chelating.[23, 39-41] For example, our group has certified the much better defect passivation effect of multi-active-site ligand compared with the corresponding single-active-site ligands.[23] Li et al. passivated the defects at GBs by using a polymeric room-temperature molten salt poly(1-vinyl-3-ethyl-acetate) imidazole tetrafluoroborate (PEa) with multiple chemical anchoring sites and enhanced device photovoltaic performance.[39] Certainly, it needs to be pointed out that proper spatial

conformation should be required to guarantee the simultaneous chemical anchoring of multiple functional groups on the surface of perovskite films.[23] It is worth noting that it is one effective strategy to increase defect passivation effect by enriching chemical bonding modes. It was extensively testified that multiple chemical interaction modes including coordination bonding, hydrogen bonding and ionic bonding were accomplished through employing different functional groups (e.g., -COOH and F) to functionalize organic salts.[29, 30, 42] In short, functional groups and spatial conformation modulations are equally important for the realization of multi-active-site anchoring and multiple chemical bonding, which maximizes defect passivation effect and minimizes interfacial nonradiative recombination losses.

In this work, we developed an effective interfacial defect and carrier management strategy by synergistically modulating organic functional groups and spatial conformation of organic ammonium salt modification molecules. This strategy was implemented by employing propylammonium ions (PAI), 3-ammonium propionic acid iodide (3-APAI) and 5-aminopentanoic acid hydroiodide (5-AVAI) to treat the surface of 3D perovskite films. It was revealed experimentally that 2D perovskite passivation layers were formed for PAI and 5-AVAI while no 2D perovskites were generated for 3-APAI even if high concentration was used. The organic ammonium salt 3-APAI exhibited much better defect passivation effect than 2D perovskite layers formed PAI and 5-AVAI. COOH groups in 3-APAI and 5-AVAI can

form hydrogen bonding with Formamidinium (FA^+) and form coordination bonding with undercoordinated Pb^{2+}, which contributed to their better defect passivation effect as compared to PAI without COOH. It was demonstrated theoretically that COOH and NH_3^+ at both ends of 5-AVA^+ can not simultaneously interact with perovskites due to too long alkyl chain. In contrast, COOH and NH_3^+ at both ends of 3-APA^+ can be simultaneously chemically anchored on the surface of perovskite films because of appropriate alkyl chain length, which strengthened defect passivation effect. COOH and NH_3^+ in 3-APAI can synergistically passivate positively and negatively charged defects by multiple chemical bonds including hydrogen bonding, coordination bonding and ionic bonding. As a result, defect density was gradually depressed and carrier lifetime was gradually increased in the order of control, PAI, 3-APAI and 5-AVAI. The 3-APAI treatment enables the realization of interfacial defect passivation, interfacial energy band alignment modulation, and interfacial carrier dynamics enhancement, resulting in enhanced efficiency, suppressed hysteresis and significantly improved stability. Among the investigated modifiers, the device with 3-APAI showed the highest PCE up to 24.72% (certified 23.68%), which is among the highest efficiencies hitherto reported for the devices fabricated without antisolvents. At the same time, the encapsulated 3-APAI-modified device maintained 96.1% of its initial PCE after 1400 h of operation under one sun continuous illumination. The present work highlights the significance of managing interfacial defects and carriers by synergistically modulating

functional groups and spatial conformation of modification molecules in order to minimize interfacial nonradiative recombination losses.

2. Results and Discussion

2.1 Molecular Dynamics Simulation

The perovskite films were fabricated as described in the experimental section. In this work, perovskite precursor solution was spin-coated on SnO_2 films during which no antisolvent was employed. The vacuum flash technology was adopted to promote the perovskite crystallization. To improve the quality of perovskite films and facilitate interfacial charge extraction, three organic ammonium salt molecules (PAI, 3-APAI and 5-AVAI) were selected to modify the interface between perovskite layer and hole transport layer (HTL). **Figure 1**a shows the chemical structures of PAI, 3-APAI and 5-AVAI. Obviously, all molecules have the same cation functional group ($-NH_3^+$) and anion (I^-). Among them, $-NH_3^+$ was expected to be able to form 2D perovskites[26] or passivate cation vacancy defects via ionic bonding and hydrogen bonding[32, 43]. Meanwhile, it was anticipated that I^- can passivate iodide vacancy defects. Except for $-NH_3^+$, 3-APAI and 5-AVAI possess a -COOH functional group. We speculated that -COOH is capable of healing uncoordinated Pb^{2+} defects via coordination bonding and can suppress the migration of FA^+ by hydrogen bonding.[23, 44] It

was posited that -COOH and -NH_3^+ can be simultaneously firmly anchored on the surface of perovskite films if the spatial conformation induced by the different distance between -COOH and -NH_3^+ is suitable. The above molecular design helps us understand how functional groups and spatial conformation have an impact on defect passivation effect and interfacial carrier dynamics by affecting the formation of 2D perovskites and chemical adsorbing modes.

Ab initio molecular dynamics (AIMD) simulations were performed to theoretically explore whether as-used organic ammonium salts can form 2D perovskites and how they passivate the defects at the surface of perovskite films as well as the effect of spatial conformation on defect passivation effect. For the PAI molecules, the -NH_3^+ groups were inserted into the FA vacancies and then accordingly, the 2D perovskite was formed, as exhibited in Figure 1b. 2D perovskite was also generated for the 5-AVAI (Figure 1c). However, the situation changed when the 3-APAI molecules were adsorbed on the perovskite surface. The simulation results in Figure 1d show that the PbI_6 octahedrons are over-distorted after adsorbing 3-APAI molecules such that the 2D perovskite is tough to form, which is consistent with the experimental findings that 2D perovskite is formed easily for PAI and 5-AVAI, but not for the 3-APAI. This suggests that the -COOH group and the distance between it and -NH_3^+ have a profound impact on the possibility of the formation of

2D perovskites. When the distance is too long just as 5-AVAI, it is impossible that -COOH and -NH_3^+ groups simultaneously interact with perovskites. In comparison, the appropriate distance guarantees that -COOH and -NH_3^+ groups can be simultaneously chemically anchored on the surface of perovskites. Subsequently, in order to gain insights into the defect passivation mechanisms and effects with these organic ammonium salts, we constructed a $FAPbI_3$ supercell with mixed defects (FA vacancy and uncoordinated Pb) and performed the AIMD simulations again **(**Figure 1e). To investigate the complex behaviours of the passivation molecules at room temperature, the -NH_3^+ groups were let to face down and the -COOH groups to face up (Figure 1f). At the beginning of the simulation, nine molecules were put on the surface of perovskites. After 10 ps molecule dynamic simulations, the PAI molecules were found to not be able to form stable adsorption (Figure 1g), and two of the nine molecules escaped from the perovskite surface (Figure S1, Supporting Information), resulting in a poor defect passivation effect. By contrast, the 5-AVAI molecules formed stable adsorption on the perovskite surface, in which the FA vacancies were fully occupied by the -NH_3^+ groups of 5-AVAI (Figure 1h). Nevertheless, no Pb-O bonding could be observed. This implies that too long alkyl chain is not conducive to simultaneous interaction and anchoring of -COOH and -NH_3^+ groups on the surface of perovskites. It also indicates that -NH_3^+ group is much easier to interact with perovskites compared with -COOH. Under the circumstances**,** appropriate spatial conformation is required to ensure simultaneous chemical anchoring of -

COOH and -NH_3^+ groups on the surface of perovskites. Figure 1i shows the final configuration of the 3-APAI molecules adsorbed on perovskite after the molecular dynamic simulation. The 3-APAI molecules formed not only stable adsorption but also the Pb-O bonding. In such a way, both the FA vacancy and uncoordinated Pb defects were effectively passivated after 3-APAI modification. It can be clearly seen in Figure 1j that 3-APAI had the highest binding energy (E_b) with perovskites with different defect types among all passivators, suggesting that 3-APAI can simultaneously passivate multiple defects and exhibited the best passivation effect for various defects. As we expected, 3-APAI treatment enabled the lowest defect density and longest carrier lifetime of the corresponding modified perovskite films, which should be responsible for the best performance for the 3-APAI-modified device among all devices.

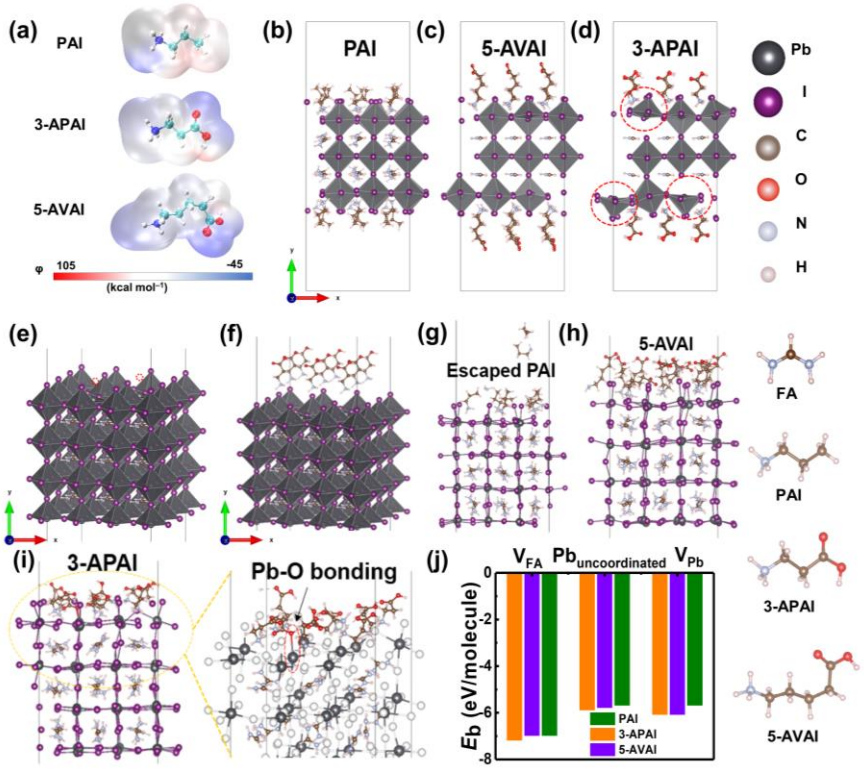

Figure 1. a) Molecular structures of PAI, 3-APAI and 5-AVAI. Optimized structures of the 2D perovskites based on b) PAI, c) 5-AVAI and d) 3-APAI. The circle regions represent the over-distorted PbI_6 octahedrons induced by 3-APAI. e) $FAPbI_3$ surface slab with mixed defects of FA and I vacancies. The circle is used to indicate the missing of I atoms. f) The initial structure before optimization where the -COOH groups face up and the $-NH_3$ groups face down. g) Structure with PAI absorption after 10 ps molecular dynamic simulation. Two from adsorbed nine PAI molecules are found to escape from surface. h) Structure with adsorbed 5-AVAI molecules at the end of 10 ps molecular dynamic simulation. i) Final configuration of the 3-APAI molecules after molecular dynamic simulation. The enlarged

area shows one 3-APAI molecule flips and forms Pb-O bonding. j) Binding energies (E_b) between different ammonium salt molecules and perovskites with various defects.

2.2 Structural and Morphology Characterization of the Perovskite Films

In order to testify the reliability of theoretical calculation results, we carried out X-ray diffraction (XRD) and grazing incidence wide-angle X-ray scattering (GIWAXS) measurements to confirm whether these organic ammonium salts treatment produced 2D passivation layer. **Figure 2**a illustrates XRD patterns of the perovskite films treated by 20 mg/mL of PAI, 3-APAI and 5-AVAI solutions. All perovskite films exhibited two strong diffraction peaks at about 14.1° and 28.3°, which was indicative of highly crystalline perovskite films required for efficient and stable PSCs. For PAI-modified perovskite film, two new characteristic diffraction peaks at 4.8° and 9.6° arose, which is ascribed to the formation of 2D perovskite. The generated 2D perovskite was $(PA)_2FA_2Pb_3I_7$ as evidenced by the results in Figure S2 in the Supporting Information. In case of 5-AVAI-modified perovskite film, a new diffraction peak at 5.7° verified the formation of 2D perovskite and generated 2D perovskite was $(5\text{-}AVA)_2PbI_4$ as revealed in Figure S3 in the Supporting Information. Therefore, PAI and 5-AVAI modification led to forming 2D/3D heterojunction, which can result in a favorable type-II band alignment.[26] However, 2D perovskite is not beneficial for

carrier transport.[35] Interestingly, we did not observe the diffraction peaks of 2D or low-dimensional perovskites upon 3-APAI treatment even if the concentration was increased to 80 mg/mL (Figure S4 and S5, Supporting Information). These results indicate that 2D perovskite was formed for PAI and 5-AVAI treatment whereas no 2D perovskite cannot be generated for 3-APAI, which is in accordance with the above theoretical results. Because of appropriate spatial conformation, -COOH and $-NH_3^+$ groups in 3-APAI can be firmly anchored on the surface of perovskite films, which made the formation of 2D perovskite difficult. For PAI and 5-AVAI, $-NH_3^+$ group at one side of molecules face down and the $-CH_3$ or -COOH face up, which is beneficial to form 2D perovskites. From GIWAXS results in Figure 2b-c, we observed a new sharp and discrete Bragg spot at q_z of ~0.5 in PAI-treated perovskite film in comparison with the control perovskite film, confirming the formation of 2D perovskite $(PA)_2FA_2Pb_3I_7$. For 3-APAI-treated film, no new Bragg spot appeared (Figure 2d), showing that no 2D perovskites were generated. A new sharp and discrete Bragg spot at q_z of ~0.4 was perceived for 5-AVAI-treated film with respect to the control film, demonstrating the generation of 2D perovskite $(5\text{-}AVA)_2PbI_4$. The results again confirmed that 2D perovskites can be formed after the treatment of PAI and 5-AVAI while 3-APAI treatment can not result in the formation of 2D perovskite due to the synergistic effect of functional groups and spatial conformation.

We performed top-view scanning electron microscope (SEM) measurements to study the morphology of the perovskite films without and with modifier treatment. As presented in Figure S6 in the Supporting Information, grain sizes were maintained after surface treatment while surface morphology seems to be slightly changed as revealed by a very thin passivation layer on the surface of 3D perovskite films when we look closely.

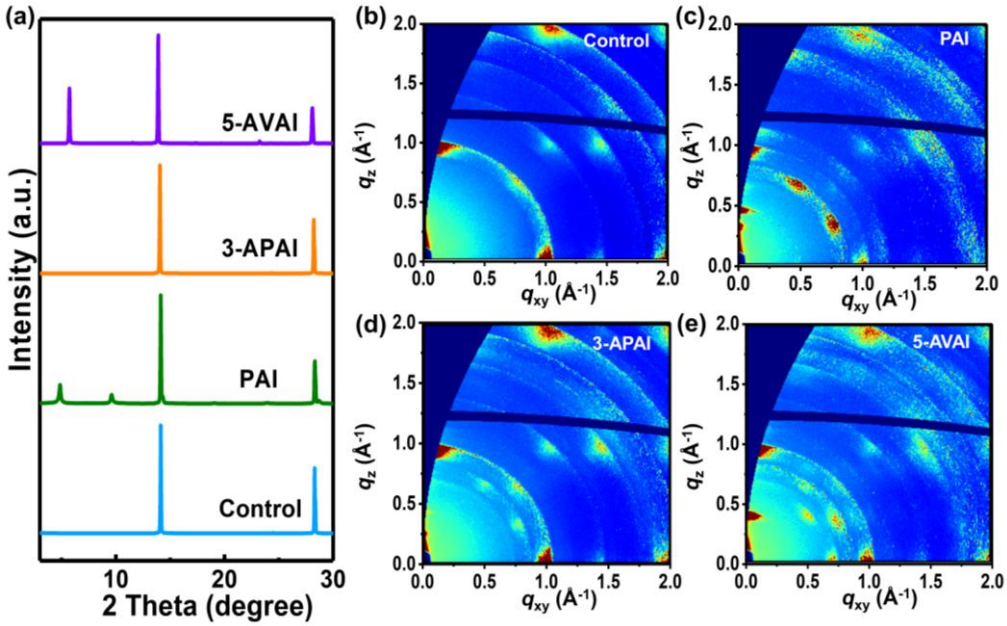

Figure 2. a) XRD patterns of the perovskite films treated by high concentration of PAI, 3-APAI and 5-AVAI (20 mg/mL). GIWAXS of the b) control, c) PAI, d) 3-APAI and e) 5-AVAI modified perovskite films (the concentration of modifiers is 20 mg/mL).

2.3 Interfacial energy level regulation

The surface electronic properties of the films were assessed by the contact potential difference (CPD) from Kelvin probe force microscopy (KPFM).[45] The CPD is defined as difference between the work function of tip (Φ_{tip}) and that of sample (Φ_{sample})[46]. The CPD value (V_{CPD}) between the tip and the sample is defined as[47]:

$$V_{CPD} = (\Phi_{tip} - \Phi_{sample})/-e$$

The KPFM images of the control and modified perovskite films are shown in **Figure 3**a-d. It can be seen in Figure 3e that the average CPD value of the control and PAI, 3-APAI and 5-AVAI modified perovskite films is −180.18, −201.37, −274.91, and −241.01 mV, respectively. Since the KPFM measurement uses zero potential methods to record the volt potential value[48], we could deduce that the work function of perovskite surface upshifts 0.094 V after 3-APAI treatment[47], which is in line with enhanced V_{OC} of the 3-APAI-modified devices.

We carried out ultraviolet photoelectron spectroscopy (UPS) measurements to study the surface electronic structures of the perovskite films. Figure S7 in the Supporting Information shows the UPS spectra of the control and modified perovskite films. Through UPS (Figure S7) and the optical band gap (E_g) obtained from the UV-vis absorption starting point (Figure S8, Supporting Information), the valence band maximum (E_{VB}) and conduction band minimum (E_{CB}) were calculated, which were plotted in Figure 3f. Obviously, E_{VB} values were upshifted after the modification of PAI, 3-APAI and 5-AVAI, which is indicative of

reduced energy offset between perovskite film and Spiro-OMeTAD. The 3-APAI modification achieved a smallest energy offset, which should contribute to the most efficient hole extraction.

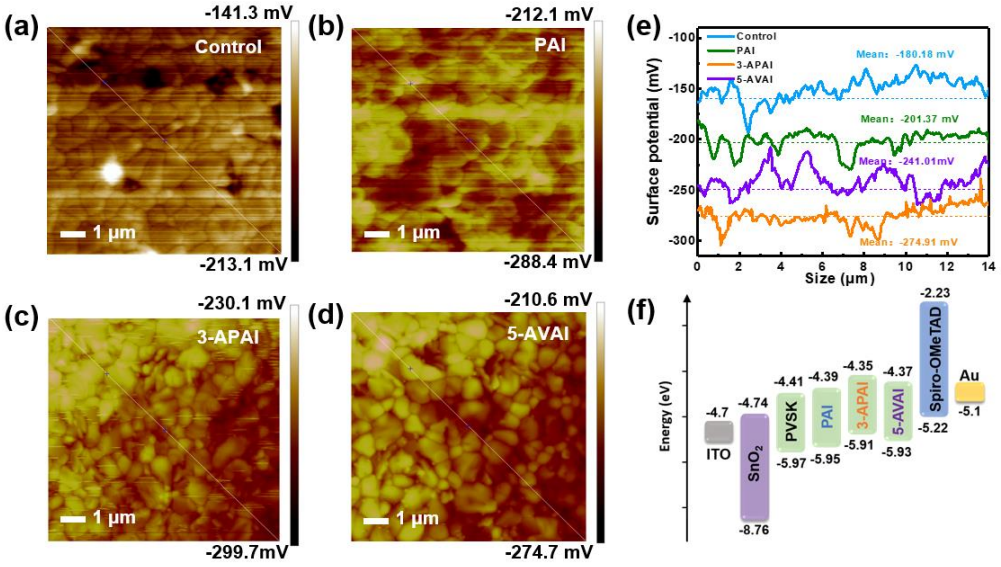

Figure 3. KPFM of the a) control and b) PAI, c) 3-APAI and d) 5-AVAI modified perovskite films. e) Contact potential difference along the lines in (a)-(d). f) UPS spectra of perovskite films. (left) Femi edge ($E_{F\text{-edge}}$), and (right) cut-off energy ($E_{cut\text{-}off}$). g) Energy level diagrams of the control and PAI, 3-APAI and 5-AVAI modified perovskite films.

2.4 Investigation of Interfacial Carrier Dynamics

To investigate the effect of interface modification on carrier recombination, we performed steady-state photoluminescence (SSPL) and time-resolved photoluminescence (TRPL) spectra measurements for the control and modified perovskite films deposited on non-conductive glass substrates with Spiro-OMeTAD as the hole carrier extracting layer. After the perovskite films were in contact with the Spiro-OMeTAD, notably reduced PL intensity was observed for all samples (**Figure 4**a). The strongest PL quenching was realized for 3-APAI treated sample. The carrier lifetimes of the control, PAI-, 3-APAI-, and 5-AVAI-modified perovskite films were 959.13, 724.36, 488.43 and 577.40 ns, respectively (Figure 4b and Table S1, Supporting Information). It indicates that 3-APAI-modified perovskite film exhibited the shortest carrier lifetime among investigated samples, which is beneficial for hole extraction and transfer. The transient reflection spectroscopy (TRS) with an excitation of 2.58, 2.07, and 1.65 eV pump pulses was measured to quantify surface extraction velocity (SEV) (Figure 4c-f). Compared with the control sample (10 cm/s), the PAI (107.8±209.1 cm/s), 3-APAI (1425.2±242.2 cm/s), and 5-AVAI (1089.1±193.8 cm/s) modified samples possessed a much increased SEV value, suggesting that hole extraction was facilitated after interface modification. The fastest hole extraction was realized for 3-APAI treated sample, which is attributed to the optimal defect passivation effect and the smallest hole extraction barrier. The synergistic effect of functional groups and appropriate spatial conformation can well account for the most efficient hole extraction and transfer upon the treatment of 3-APAI.

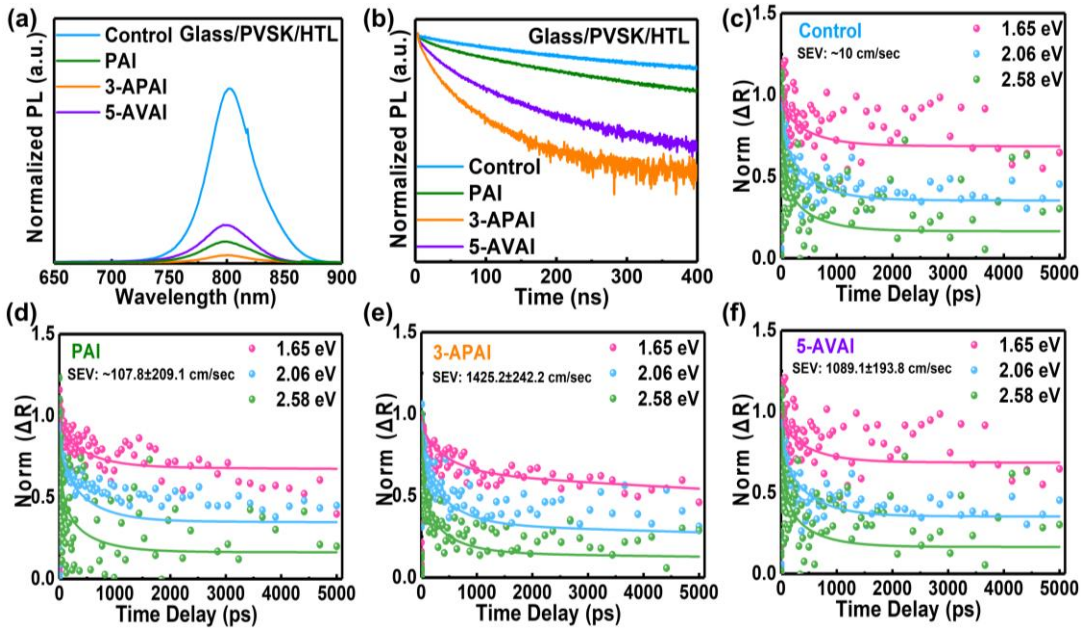

Figure 4. a) PL and b) TRPL spectra for the control and modified perovskite films with HTL. Transient reflection kinetics of the c) pristine and d) PAI, e) 3-APAI, and f) 5-AVAI treated perovskite films with HTL.

2.5 Defect Passivation Investigation

Since no 2D perovskite was formed for 3-APAI treatment, we investigated the chemical interaction mechanisms between 3-APAI and perovskites by carrying out X-ray photoelectron spectroscopy (XPS) and Fourier-transform infrared (FTIR) spectroscopy measurements. As displayed in Figure S9a in the Supporting Information, the two peaks at 142.67 and 137.77 eV in the control perovskite film were attributed to Pb $4f_{5/2}$ and Pb $4f_{7/2}$,

respectively, which were shifted to higher binding energies after 3-APAI modification (142.86 and 137.98 eV), indicating the coordination bonding between -COOH and undercoordinated Pb^{2+} and/or ionic bonding of $-NH_3^+$ with PbI_6^{4-} octahedron[44, 49-51]. Figure S9b in the Supporting Information showed that the binding energies of I $3d_{3/2}$ (630.33 eV) and I $3d_{5/2}$ (618.89 eV) in the control perovskite film were moved to higher values of 630.53 and 618.99 eV for the 3-APAI-modified perovskite film, which should be put down to the hydrogen bonding of $-NH_3^+$ and/or -COOH with I^-[52-54]. From Figure S9c in the Supporting Information, the C=O stretching vibration peak of 3APAI was shifted from 1642 cm^{-1} to 1610 cm^{-1} after mixing with PbI_2, which is indicative of the coordination interaction between -COOH and Pb^{2+}. The above results manifest that the two functional groups -COOH and $-NH_3^+$ can simultaneously chemically interact with perovskites by coordinating bonding, hydrogen bonding and ionic bonding, which is in line with the theoretical calculation results. The simultaneous interaction of -COOH and $-NH_3^+$ with perovskites makes the formation of 2D perovskite impossible. The synergistic interaction of -COOH and $-NH_3^+$ groups were anticipated to be able to fully passivate various interfacial defects (e.g., FA vacancy, undercoordinated Pb^{2+}, Pb^{2+} vacancy, halide vacancy and PbI_3^- antisite).

The positron annihilation spectroscopy (PAS) is a very powerful technique for characterizing the chemical nature of lattice defects.[55] Since positively charged positrons

are antiparticles of the electrons, one can quantify the negatively charged defects through PAS technique. In our case, FA vacancy, Pb vacancy and PbI_3^- antisite defects could be simultaneously present at perovskite film surface. Therefore, we measured the positron annihilation lifetime spectra of the control and modified perovskite films (**Figure 5**a). The lifetime spectra were fitted by three-component fitting. The shortest component (τ_1) signifies the free annihilation of the positron in the bulk of the perovskite. The intermediate component (τ_2) stands for the positron lifetime at the defect site and its intensity denotes the relative number of defects in perovskite films. The longest component (τ_3) is because of formation of positronium high-dimensional defects (i.e., grain boundary and large voids). It can be observed obviously in Table S2 in the Supporting Information that the τ_2 values were diminished after 3-APAI treatment (733 ps) compared with the pristine film (740 ps). Simultaneously, the intensity of the intermediate lifetime component (I_2) kept the same trend as τ_2. It indicates that negatively charged defect density was decreased after 3-APAI modification, which is due to its effective passivation for FA vacancy, Pb vacancy and PbI_3^- antisite defects.

We also carried out steady state PL and TRPL tests for the perovskite thin films without Spiro-OMeTAD to analyze the carrier radiative recombination processes. PL intensity was increased incessantly in the order of control, PAI, 5-AVAI and 3-APAI modified perovskite

films (Figure S10, Supporting Information). Meanwhile, the TRPL curves in Figure 5b were fitted by double exponential function and the fitted results are illustrated in Table S3 in the Supporting Information. It can be seen evidently that the PAI (350.04 ns), 5-AVAI (382.98 ns) and 3-APAI (491.31 ns) modified perovskite films showed longer average carrier lifetimes than the bare perovskite film (303.01 ns), indicating that the defects on the surface of perovskite films were effectively passivated after modification. Among all samples, 3-APAI modified perovskite film demonstrated a longest carrier lifetime, suggesting that 3-APAI salt had much better defect passivation effect as compared to the 2D perovskites induced by PAI and 5-AVAI treatment. It was previously reported that organic salt was more effective in passivating interfacial defects than the corresponding 2D perovskite.[43] This shows that defect passivation effect of modifiers can be heightened through modulating the organic functional groups and spatial conformation.

2.6 Carrier Recombination Analysis of Devices

Subsequently, we studied the carrier recombination of the control and modified PSCs. The built-in potential (V_{bi}) was obtained from Mott−Schottky plots in Figure 5c. It is well known that V_{OC} is positively correlated with V_{bi}.[56] Compared with the control device (1.030 V), the PSCs treated with PAI, 3-APAI and 5-AVAI delivered a higher V_{bi} of 1.038V, 1.065 V and 1.053V, respectively. This suggests that hole separation and extraction were promoted

after surface modification. Moreover, the optimal hole separation and extraction was observed in APAI-modified device, which should be owing to its smallest hole extraction barrier and most effective defect passivation. As a result of much inhibited nonradiative recombination due to effective defect passivation and advantageous energy band alignment, the dark current was decreased after interface modification but the 3-APAI modified device exhibited the lowest leakage current (Figure S11, Supporting Information). As presented in Figure 5d, the ideality factor *m* (1.16) of the 3-APAI modified device is closer to 1 than those of the control (1.63), PAI (1.58) and 5-AVAI (1.30) treated devices, indicating that 3-APAI treatment is the most effective in suppressing interfacial nonradiative recombination.

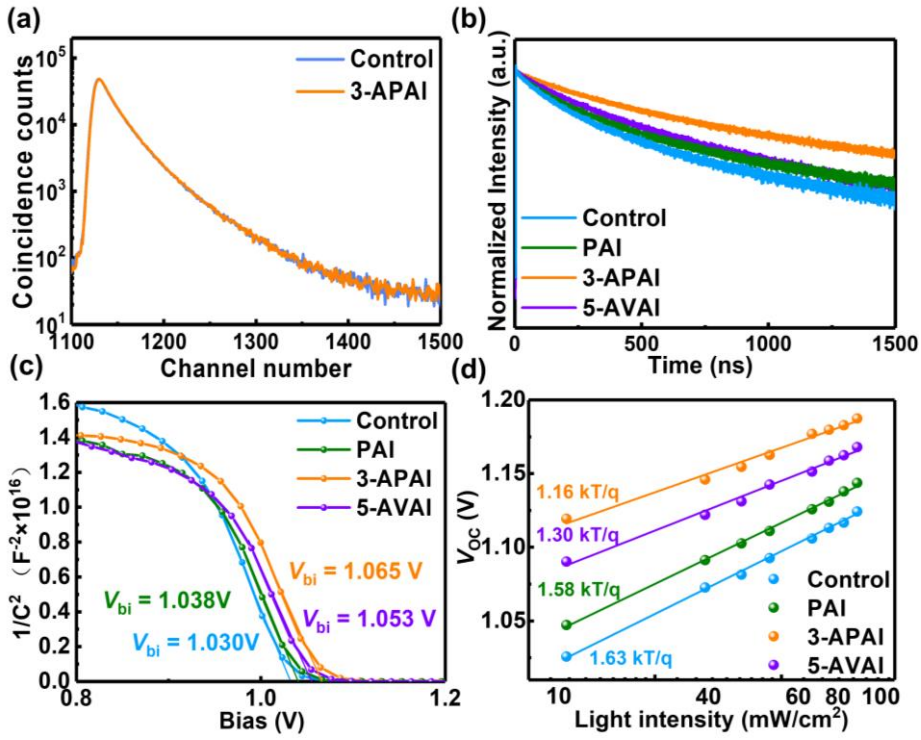

Figure 5. a) Typical positron lifetime spectra for the control and modified perovskite films. b) TRPL spectra of the control and modified perovskite films deposited on glass substrate. c) Mott-Schottky plots of the control and modified PSCs. d) V_{OC} as a function of light intensities for the control and PAI, 3-APAI and 5-AVAI treated PSCs.

2.7 Photovoltaic Performance

We constructed planar PSCs without and with interface modifiers and the device configuration is exhibited in the cross-sectional SEM (Figure S12**,** Supporting Information**)**. Figure S13-S15 in the Supporting Information demonstrated that the optimal concentrations of PAI, 3-APAI, and 5-AVAI were 2.0, 3.0 and 3.5 mg/mL, respectively. **Figure 6**a compares the photovoltaic parameters of the control and modified devices with the optimal concentration of PAI, 3-APAI, and 5-AVAI. Compared with the control devices, PAI, 3-APAI, and 5-AVAI treated PSCs achieved improved average PCE values as a result of enhanced all photovoltaic parameters, especially for V_{OC} and FF, which is attributed to reduced defect density, increased carrier lifetimes and inhibited interfacial nonradiative recombination. The devices with 3-APAI and 5-AVAI possessed better device performance in comparison with the devices with PAI, showing that -COOH group had a positive impact on surface defect passivation. Among the investigated three passivators, 3-APAI demonstrated the best device

performance. On the one hand, this indicates that organic salts could be more effective in defect passivation than 2D perovskite. On the other hand, the synergistic chemical anchoring of organic functional groups upon appropriate spatial conformation is conducive to maximizing defect passivation effect and minimizing interfacial nonradiative recombination. The *J-V* curves of the champion control and modified PSCs are presented in Figure 6b-e. The control device obtained a peak PCE of 22.10% with a J_{SC} of 25.54 mA cm^{-2}, a V_{OC} of 1.12 V, and an FF of 77.25%. In contrast, the PAI and 5-AVAI modified devices realized improved maximum PCEs of 22.68% (a J_{SC} of 25.41 mA cm^{-2}, a V_{OC} of 1.14 V, and an FF of 78.49%) and 23.12% (a J_{SC} of 25.46 mA cm^{-2}, a V_{OC} of 1.13 V, and an FF of 80.36%), respectively. Particularly, the champion device with 3-APAI achieved an appealing PCE of 24.72% (a J_{SC} of 25.59 mA cm^{-2}, a V_{OC} of 1.19 V, and an FF of 81.20%), to the best of our knowledge, which is among the highest PCEs reported for the PSCs without antisolvents up to now (Table S4, Supporting Information). More importantly, we achieve an attractive certified PCE of 23.68% with a J_{SC} of 25.72 mA/cm^2, a V_{OC} of 1.168 V, and an FF of 78.84% (Figure S16-19, Supporting Information).

For all devices, hysteresis index (HI) was calculated according to the formula of HI = ($PCE_{Reverse} - PCE_{Forward}$)/$PCE_{Reverse}$). The HI values were 8.8%, 8.1%, 1.2% and 8.3% for the control, PAI, 3-APAI and 5-AVAI modified devices, respectively. The 3-APAI based devices

exhibited the smallest hysteresis among all investigated devices. Reduced defect density and ameliorated interfacial charge extraction should be chiefly responsible for repressed hysteresis.[1, 57, 58] Besides, suppressed ion migration due to the effective passivation of FA^+ and I^- vacancies also should be one of important reasons for mitigated hysteresis because vacancy defects can provide pathways for ion migration.[1]

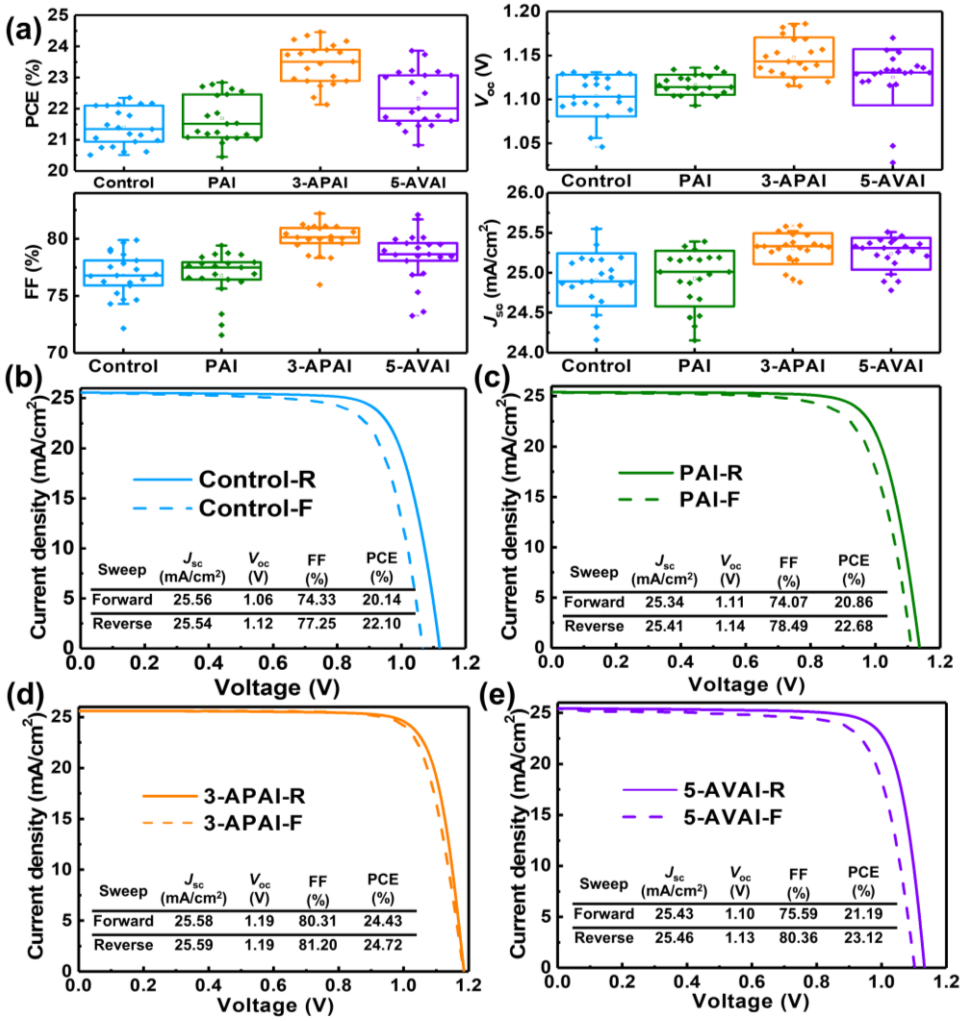

Figure 6. a) Statistical photovoltaic parameters of the control and modified devices. *J-V* curves

of the best-performing b) control, c) PAI, d) 3-APAI and e) 5-AVAI modified devices.

2.8 Long-Term Stability

Since long-term stability plays a decisive role in final commercial application of PSCs, we gained insights into the effect of interface modification on the long-term stability of the control and modified films and devices. We recorded optical photographs of the control and 3-APAI modified perovskite films stored in an airtight container with a humidity of 75±10% in the dark at room temperature. From Figure S20 in the Supporting Information, the control perovskite film decomposed obviously after 5 days while the 3-APAI modified perovskite films still kept black under the same aging time. After 10 days of aging, significant degradation can be noticed for the whole control film whereas just slight degradation happened on the edge of the perovskite film with 3-APAI. This indicates that moisture resistance of perovskite films was prominently strengthened after 3-APAI modification. This is because the -COOH and $-NH_3^+$ groups at both ends of 3-APAI molecules were firmly chemically anchored on the surface of perovskite films and simultaneously the alkyl chain between functional groups can suppress or block water invasion. This suggests that synergistic effect of functional groups and spatial conformation is beneficial for enhancing not only PCE but also stability.

Furthermore, XRD measurements were conducted to explore the moisture stability of the control and 3-APAI modified perovskite films. It can be found easily in Figure S21 in the Supporting Information that the intensity of main diffraction peaks of 3D perovskite for the control perovskite films reduced after aging for 10 days, diffraction peak intensity of PbI_2 markedly increased, and yellow non-perovskite phase emerged. In stark contrast, the intensity of main diffraction peaks of 3D perovskite was almost maintained for the 3-APAI modified perovskite films and no yellow non-perovskite phase was observed under the same aging condition. In short, 3-APAI modification remarkably enhanced moisture resistance of perovskite films by effective defect passivation and hydrophobic alkyl chain. We have observed from Figure S22 in the Supporting Information that the morphology of the control perovskite film has been spoiled while no evident morphology change occurred for the 3-APAI-modified perovskite film, which again proved the enhanced moisture stability after 3-APAI treatment.

We evaluated the long-term operational stability of the encapsulated control and modified devices under continuous illumination of 100 mW/cm^2 white light LED (Figure 7 and Figure S23, Supporting Information). The control device degraded rapidly, which was confirmed by retaining 56.2% (from 20.07% to 11.29%) of its initial efficiency value after 1400 hours. In comparison, the PAI, 3-APAI and 5-AVAI modified devices exhibited much

improved photostability, which was evidenced by maintaining 70.1% (from 22.85% to 16.18%), 96.1% (from 23.73% to 22.81%) and 87.8% (from 23.02% to 20.23%) of their original PCE values after 1400 hours of light stress, respectively. The improved light stability should be ascribed to suppressed trap-assisted nonradiative recombination, inhibited ion migration, and reinforced interfacial contact.[1, 9, 23, 30] It is worth stressing that the 3-APAI modified devices demonstrated the most outstanding stability, which is owing to the simultaneous chemical anchoring of -COOH and $-NH_3^+$ groups on the perovskite film surface. This again highlights the significance of the synergistic modulation of functional groups and spatial conformation in managing interfacial defects and carrier dynamics toward the realization of stable and efficient perovskite photovoltaics. Previous studies have revealed that multidentate ligand chelation can strengthen the chemical interaction between modification molecules and perovskites and thereby prominently enhance stability and PCE.[23, 39-41, 59, 60]

The moisture stability was studied by exposing the unencapsulated control and 3-APAI-modified devices in an ambient environment with a 35±5% RH. Figure S24 in the Supporting Information manifests that the control device degraded to 57.2% of its initial PCE after 2000 hours of aging, while the device with 3-APAI treatment degraded to 90.1% of its initial PCE under the same aging condition, indicating improved moisture resistance after 3-APAI

modification, which is in keeping with ameliorated film moisture stability. As for the thermal stability of PSCs, the encapsulated devices were aged at 100 °C in air ambient conditions. After heating for 108 h, 79.7% of their initial efficiencies were retained for 3-APAI modified devices, while 60.1% of their efficiencies were maintained for the control device, as exhibited in **Figure S25**. In conclusion, we have attested that synergistic modulation of functional groups and spatial conformation of modifiers is a feasible and practical approach to managing interfacial defects and carriers to achieve high-performance PSCs.

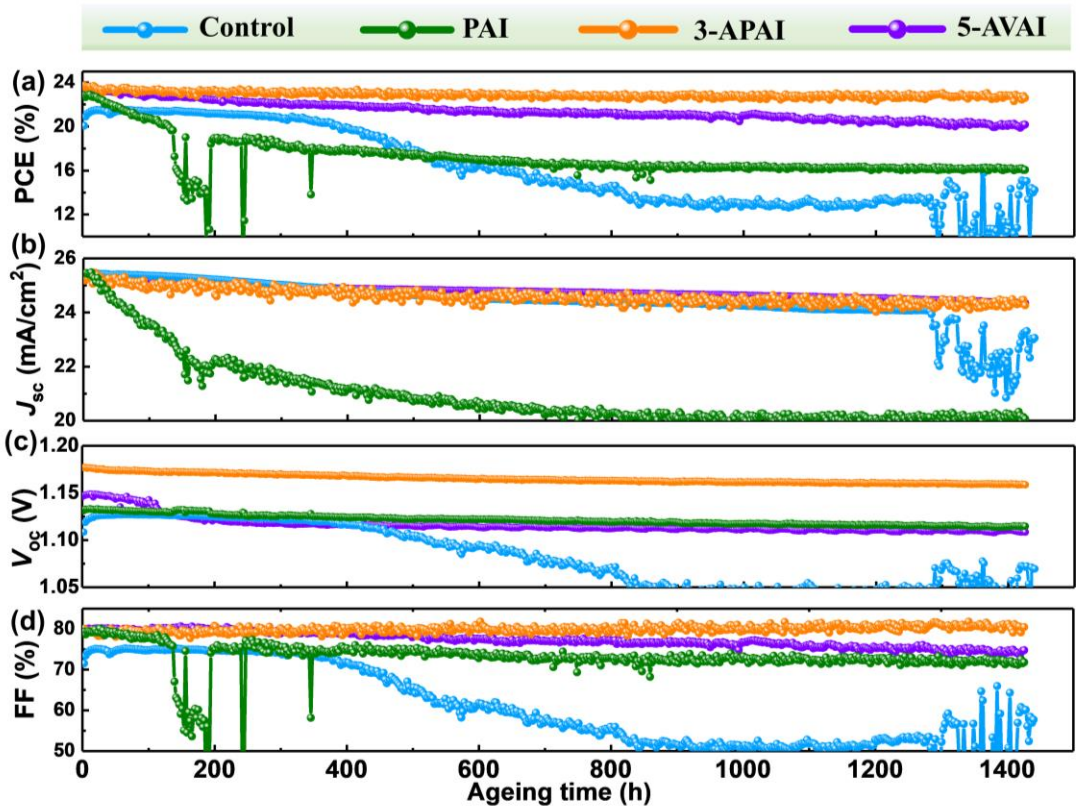

Figure 7. The a) PCE, b) J_{SC}, c) V_{OC} and d) FF evolution of the encapsulated control and

modified PSCs under continuous one sun illumination of 100 mW/cm^2 provided by white light LED.

3. Conclusions

In summary, we effectively managed interfacial defect and carrier dynamics by synergistic modulation of functional groups and spatial conformation of organic ammonium salt modification molecules. PAI, 3-APAI and 5-AVAI were adopted to treat the surface of perovskite films. PAI and 5-AVAI post-treatment resulted in the formation of 2D perovskite passivation layers while 2D perovskite can not be generated after 3-APAI treatment. Due to appropriate alkyl chain length, -COOH and -NH_3^+ groups at both ends of 3-APAI molecules can be simultaneously chemically anchored on the surface of perovskite films via coordinating bonding with undercoordinated Pb^{2+} and ionic bonding and hydrogen bonding with octahedron PbI_6^{4-}, respectively, which strengthened defect passivation effect and improved interfacial carrier extraction and transfer. It was revealed that 3-APAI molecules can passivate anionic and cationic defects by multiple chemical bonds. Therefore, the much better defect passivation effect was demonstrated for 3-APAI than 2D perovskite layers formed by PAI and 5-AVAI. Impressively, the 3-APAI modified device based on vacuum flash method produced a promising PCE as high as

24.72% (certified 23.68%), which is one of the highest efficiencies ever reported for the devices fabricated without antisolvents. Moreover, the encapsulated 3-APAI-modified device maintained 96.1% of its initial PCE after 1400 h of light stress under one sun continuous illumination. This work provides a simple and effective strategy to minimize interfacial nonradiative recombination losses by synergistically modulating functional groups and spatial conformation of modification molecules.

Supporting Information

Supporting Information is available from the Wiley Online Library or from the author.

Author Contributions

D. G., R. L. and X. C. contributed equally to this work. D. G., R. L., X. C., J. C. and C. C. conceived the project and designed the experiments. J. C., C. C., L. D. and J. T., directed and supervised this project. D. G., R. L., X. C., C. W., B. Z., M. L. and X. S. performed experiments. X. Y., S. G., T. P. and H. Y. contributed materials and analysis tools. J. C., C. C. and D. G. wrote the manuscript. All authors discussed the results and commented on the manuscript.

Conflict of Interest

The authors declare no conflict of interest.

Data Availability Statement

Research data are not shared.

Acknowledgements

This work was supported by the Science and Technology Development Fund (FDCT), Macau SAR (No. 0018/2022/A1), the 'Macao Young Scholars Program' (Project code: AM2021013), the National Natural Science Foundation of China (62004058, U21A2076, 62274018, 21701041, 52071048, 62274117), Natural Science Foundation of Hebei Province (F2020202022), the Open Fund of the State Key Laboratory of Integrated Optoelectronics (IOSKL2020KF09), State Key Laboratory of Reliability and Intelligence of Electrical Equipment (No. EERI_PI20200005, EERI_0Y2021001), the Fundamental Research Funds for the Central Universities (2020CDJ-LHZZ-074), the Natural Science Foundation of Chongqing (cstc2020jcyj-msxmX0629), and the Support plan for Overseas Students to

Return to China for Entrepreneurship and Innovation (cx2020003). Hebei Graduate Innovation Funding Project (CXZZSS2023026, CXZZBS2023037). The authors thank Beijing Synchrotron Radiation Facility (BSRF) for GIWAX measurement.

References

[1] J. Chen, N.-G. Park, *Adv. Mater.* **2019**, *31*, 1803019.

[2] T. Zhang, F. Wang, H.-B. Kim, I.-W. Choi, C. Wang, E. Cho, R. Konefal, Y. Puttisong, K. Terado, L. Kobera, M. Chen, M. Yang, S. Bai, B. Yang, J. Suo, S.-C. Yang, X. Liu, F. Fu, H. Yoshida, W. M. Chen, J. Brus, V. Coropceanu, A. Hagfeldt, J.-L. Brédas, M. Fahlman, D. S. Kim, Z. Hu, F. Gao, *Science* **2022**, *377*, 495.

[3] Y. Zhao, F. Ma, Z. Qu, S. Yu, T. Shen, H.-X. Deng, X. Chu, X. Peng, Y. Yuan, X. Zhang, J. You, *Science* **2022**, *377*, 531.

[4] J. Jeong, M. Kim, J. Seo, H. Lu, P. Ahlawat, A. Mishra, Y. Yang, M. A. Hope, F. T. Eickemeyer, M. Kim, Y. J. Yoon, I. W. Choi, B. P. Darwich, S. J. Choi, Y. Jo, J. H. Lee, B. Walker, S. M. Zakeeruddin, L. Emsley, U. Rothlisberger, A. Hagfeldt, D. S. Kim, M. Grätzel, J. Y. Kim, *Nature* **2021**, *592*, 381.

[5] H.-S. Kim, C.-R. Lee, J.-H. Im, K.-B. Lee, T. Moehl, A. Marchioro, S.-J. Moon, R. Humphry-Baker, J.-H. Yum, J. E. Moser, M. Grätzel, N.-G. Park, *Sci. Rep.* **2012**, *2*, 591.

[6] Q. Jiang, J. Tong, Y. Xian, R. A. Kerner, S. P. Dunfield, C. Xiao, R. A. Scheidt, D. Kuciauskas, X. Wang, M. P. Hautzinger, R. Tirawat, M. C. Beard, D. P. Fenning, J. J. Berry, B. W. Larson, Y. Yan, K. Zhu, *Nature* **2022**, *611*, 278.

[7] M. Kim, J. Jeong, H. Lu, T. K. Lee, F. T. Eickemeyer, Y. Liu, I. W. Choi, S. J. Choi, Y. Jo, H.-B. Kim, S.-I. Mo, Y.-K. Kim, H. Lee, N. G. An, S. Cho, W. R. Tress, S. M. Zakeeruddin, A. Hagfeldt, J. Y. Kim, M. Grätzel, D. S. Kim, *Science* **2022**, *375*, 302.

[8] W. Hui, L. Chao, H. Lu, F. Xia, Q. Wei, Z. Su, T. Niu, L. Tao, B. Du, D. Li, Y. Wang, H. Dong, S. Zuo, B. Li, W. Shi, X. Ran, P. Li, H. Zhang, Z. Wu, C. Ran, L. Song, G. Xing, X. Gao, J. Zhang, Y. Xia, Y. Chen, W. Huang, *Science* **2021**, *371*, 1359.

[9] M. Li, H. Li, Q. Zhuang, D. He, B. Liu, C. Chen, B. Zhang, T. Pauporté, Z. Zang, J. Chen, *Angew. Chem. Int. Ed.* **2022**, *61*, e202206914.

[10] National Renewable Energy Laboratory, Best research cell efficiencies. *https://www.nrel.gov/pv/cell-efficiency.html.*

[11] T. Zhang, F. Wang, H.-B. Kim, I.-W. Choi, C. Wang, E. Cho, R. Konefal, Y. Puttisong, K. Terado, L. Kobera, M. Chen, M. Yang, S. Bai, B. Yang, J. Suo, S.-C. Yang, X. Liu, F. Fu, H. Yoshida, W. M. Chen, J. Brus, V. Coropceanu, A. Hagfeldt, J.-L. Brédas, M. Fahlman, D. S. Kim, Z. Hu, F. Gao, *Science* **2022**, *377*, 495.

[12] Q. Cao, T. Wang, J. Yang, Y. Zhang, Y. Li, X. Pu, J. Zhao, H. Chen, X. Li, I. Tojiboyev, J. Chen, L. Etgar, X. Li, *Adv. Funct. Mater.* **2022**, *32*, 2201036.

[13] J. J. Yoo, G. Seo, M. R. Chua, T. G. Park, Y. Lu, F. Rotermund, Y.-K. Kim, C. S. Moon, N. J. Jeon, J.-P. Correa-Baena, V. Bulović, S. S. Shin, M. G. Bawendi, J. Seo, *Nature* **2021**, *590*, 587.

[14] X. Li, D. Bi, C. Yi, J.-D. Décoppet, J. Luo, S. M. Zakeeruddin, A. Hagfeldt, M. Grätzel, *Science* **2016**, *353*, 58.

[15] R. Azmi, E. Ugur, A. Seitkhan, F. Aljamaan, A. S. Subbiah, J. Liu, G. T. Harrison, M. I. Nugraha, M. K. Eswaran, M. Babics, Y. Chen, F. Xu, T. G. Allen, A. u. Rehman, C.-L. Wang, T. D. Anthopoulos, U. Schwingenschlögl, M. De Bastiani, E. Aydin, S. De Wolf, *Science* **2022**, *376*, 73.

[16] R. Yuan, B. Cai, Y. Lv, X. Gao, J. Gu, Z. Fan, X. Liu, C. Yang, M. Liu, W.-H. Zhang, *Energy Environ. Sci.* **2021**, *14*, 5074.

[17] J. Chen, N.-G. J. A. E. L. Park, *ACS Energy Lett.* **2020**, *5*, 2742.

[18] Z. Ni, C. Bao, Y. Liu, Q. Jiang, W.-Q. Wu, S. Chen, X. Dai, B. Chen, B. Hartweg, Z. Yu, Z. Holman, J. Huang, *Science* **2020**, *367*, 1352.

[19] M. Stolterfoht, C. M. Wolff, J. A. Márquez, S. Zhang, C. J. Hages, D. Rothhardt, S. Albrecht, P. L. Burn, P. Meredith, T. Unold, D. Neher, *Nat. Energy* **2018**, *3*, 847.

[20] L. K. Ono, S. Liu, Y. J. A. C. I. E. Qi, *Angew. Chem. Int. Ed.* **2020**, *59*, 6676.

[21] B. Chen, P. N. Rudd, S. Yang, Y. Yuan, J. J. C. S. R. Huang, *Chem. Soc. Rev.* **2019**, *48*, 3842.

[22] J. Wang, K. Datta, C. H. Weijtens, M. M. Wienk, R. A. J. A. F. M. Janssen, *Adv. Funct. Mater.* **2019**, *29*, 1905883.

[23] B. Liu, H. Bi, D. He, L. Bai, W. Wang, H. Yuan, Q. Song, P. Su, Z. Zang, T. Zhou, J. Chen, *ACS Energy Lett.* **2021**, *6*, 2526.

[24] Q. Zhou, D. He, Q. Zhuang, B. Liu, R. Li, H. Li, Z. Zhang, H. Yang, P. Zhao, Y. He, Z. Zang, J. Chen, *Adv. Funct. Mater.* **2022**, *32*, 2205507.

[25] S. Sidhik, Y. Wang, M. De Siena, R. Asadpour, A. J. Torma, T. Terlier, K. Ho, W. Li, A. B. Puthirath, X. Shuai, A. Agrawal, B. Traore, M. Jones, R. Giridharagopal, P. M. Ajayan, J. Strzalka, D. S. Ginger, C. Katan, M. A. Alam, J. Even, M. G. Kanatzidis, A. D. Mohite, *Science* **2022**, *377*, 1425.

[26] J. Chen, J.-Y. Seo, N.-G. Park, *Adv. Energy Mater.* **2018**, *8*, 1702714.

[27] H. Bi, B. Liu, D. He, L. Bai, W. Wang, Z. Zang, J. Chen, *Chem. Eng. J.* **2021**, *418*, 129375.

[28] C. Zhang, H. Wang, H. Li, Q. Zhuang, C. Gong, X. Hu, W. Cai, S. Zhao, J. Chen, Z. Zang, *J. Energy Chem.* **2021**, *63*, 452.

[29] D. Gao, L. Yang, X. Ma, X. Shang, C. Wang, M. Li, X. Zhuang, B. Zhang, H. Song, J. Chen, C. Chen, *J. Energy Chem.* **2022**, *69*, 659.

[30] D. He, T. Zhou, B. Liu, L. Bai, W. Wang, H. Yuan, C. Xu, Q. Song, D. Lee, Z. Zang, L. Ding, J. Chen, *EcoMat* **2022**, *4*, e12158.

[31] J. Chen, X. Zhao, S.-G. Kim, N.-G. Park, *Adv. Mater.* **2019**, *31*, 1902902.

[32] J. Xue, R. Wang, X. Chen, C. Yao, X. Jin, K.-L. Wang, W. Huang, T. Huang, Y. Zhao, Y. Zhai, D. Meng, S. Tan, R. Liu, Z.-K. Wang, C. Zhu, K. Zhu, M. C. Beard, Y. Yan, Y. Yang, *Science* **2021**, *371*, 636.

[33] J. Peng, D. Walter, Y. Ren, M. Tebyetekerwa, Y. Wu, T. Duong, Q. Lin, J. Li, T. Lu, M. A. Mahmud, O. L. C. Lem, S. Zhao, W. Liu, Y. Liu, H. Shen, L. Li, F. Kremer, H. T. Nguyen, D.-Y. Choi, K. J. Weber, K. R. Catchpole, T. P. White, *Science* **2021**, *371*, 390.

[34] Y. Liu, S. Akin, L. Pan, R. Uchida, N. Arora, J. V. Milić, A. Hinderhofer, F. Schreiber, A. R. Uhl, S. M. Zakeeruddin, A. Hagfeldt, M. I. Dar, M. Grätzel, *Sci. Adv.* **2019**, *5*, eaaw2543.

[35] D. Yu, F. Cao, J. Liao, B. Wang, C. Su, G. Xing, *Nat. Commun.* **2022**, *13*, 6229.

[36] X. Zuo, B. Kim, B. Liu, D. He, L. Bai, W. Wang, C. Xu, Q. Song, C. Jia, Z. Zang, D. Lee, X. Li, J. Chen, *Chem. Eng. J.* **2022**, *431*, 133209.

[37] H. Zhu, Y. Liu, F. T. Eickemeyer, L. Pan, D. Ren, M. A. Ruiz-Preciado, B. Carlsen, B. Yang, X. Dong, Z. Wang, H. Liu, S. Wang, S. M. Zakeeruddin, A. Hagfeldt, M. I. Dar, X. Li, M. Grätzel, *Adv. Mater.* **2020**, *32*, 1907757.

[38] Y. Zhang, Y. Wang, L. Zhao, X. Yang, C.-H. Hou, J. Wu, R. Su, S. Jia, J.-J. Shyue, D. Luo, P. Chen, M. Yu, Q. Li, L. Li, Q. Gong, R. Zhu, *Energy Environ. Sci.* **2021**, *14*, 6526.

[39] S. Wang, B. Yang, J. Han, Z. He, T. Li, Q. Cao, J. Yang, J. Suo, X. Li, Z. Liu, S. Liu, C. Tang, A. Hagfeldt, *Energy Environ. Sci.* **2020**, *13*, 5068.

[40] J. Liang, C. Chen, X. Hu, Z. Chen, X. Zheng, J. Li, H. Wang, F. Ye, M. Xiao, Z. Lu, Y. Xu, S. Zhang, R. Yu, C. Tao, G. Fang, *ACS Appl. Mater. Interfaces* **2020**, *12*, 48458.

[41] Q. Cao, J. Yang, T. Wang, Y. Li, X. Pu, J. Zhao, Y. Zhang, H. Zhou, X. Li, X. Li, *Energy Environ. Sci.* **2021**, *14*, 5406.

[42] B. Liu, R. Li, Q. Zhuang, X. Yu, S. Gong, D. He, Q. Zhou, H. Yang, X. Chen, S. Lu, Z.-X. Xu, Z. Zang, J. Chen, *J. Energy Chem.* **2023**, *76*, 277.

[43] Q. Jiang, Y. Zhao, X. Zhang, X. Yang, Y. Chen, Z. Chu, Q. Ye, X. Li, Z. Yin, J. You, *Nat. Photonics* **2019**, *13*, 460.

[44] L. Zhu, X. Zhang, M. Li, X. Shang, K. Lei, B. Zhang, C. Chen, S. Zheng, H. Song, J. Chen, *Adv. Energy Mater.* **2021**, *11*, 2100529.

[45] P. Chen, Y. Bai, S. Wang, M. Lyu, J.-H. Yun, L. Wang, *J. Am. Chem. Soc.* **2018**, *28*, 1706923.

[46] Y. Hou, K. Wang, D. Yang, Y. Jiang, N. Yennawar, K. Wang, M. Sanghadasa, C. Wu, S. Priya, *ACS Energy Lett.* **2019**, *4*, 2646.

[47] L. Liang, H. Luo, J. Hu, H. Li, P. Gao, *Adv. Energy Mater.* **2020**, *10*.

[48] B. Jiang, B. Zhang, Y. He, Q. Peng, Z. Jiao, L. Qiao, *Corros. Sci.* **2021**, *191*.

[49] W. Cai, Y. Wang, W. Shang, J. Liu, M. Wang, Q. Dong, Y. Han, W. Li, H. Ma, P. Wang, J. Guo, Y. Shi, *Chem. Eng. J.* **2022**, DOI: 10.1016/j.cej.2022.137033.

[50] L. Xie, J. Chen, P. Vashishtha, X. Zhao, G. S. Shin, S. G. Mhaisalkar, N.-G. J. A. E. L. Park, *ACS Energy Lett.* **2019**, *4*, 2192.

[51] N. Yi, S. Wang, Z. Duan, K. Wang, Q. Song, S. J. A. M. Xiao, *Adv. Mater.* **2017**, *29*, 1701636.

[52] C. Ma, N.-G. Park, *ACS Energy Lett.* **2020**, *5*, 3268.

[53] Y.-J. Kang, S.-N. Kwon, S.-P. Cho, Y.-H. Seo, M.-J. Choi, S.-S. Kim, S.-I. Na, *ACS Energy Lett.* **2020**, *5*, 2535.

[54] T. Xu, K. Zou, S. Lv, H. Tang, Y. Zhang, Y. Chen, L. Chen, Z. Li, W. Huang, *ACS Appl. Mater. Interfaces* **2021**, *13*, 16485.

[55] J. Dhar, S. Sil, A. Dey, P. P. Ray, D. Sanyal, *J. Phys. Chem. Lett.* **2017**, *8*, 1745.

[56] K. Choi, J. Lee, H. I. Kim, C. W. Park, G.-W. Kim, H. Choi, S. Park, S. A. Park, T. Park, *Energy Environ. Sci.* **2018**, *11*, 3238.

[57] D.-H. Kang, N.-G. Park, *Adv. Mater.* **2019**, *31*, 1805214.

[58] M. Wang, Y. Lei, Y. Xu, L. Han, Z. Ci, Z. Jin, *Sol. RRL* **2020**, *4*, 2000586.

[59] J. Chen, S.-G. Kim, X. Ren, H. S. Jung, N.-G. Park, *J. Mater. Chem. A* **2019**, *7*, 4977.

[60] G. Liu, Y. Zhong, W. Feng, M. Yang, G. Yang, J. X. Zhong, T. Tian, J. B. Luo, J. Tao, S. J. A. C. Yang, *Angew. Chem. Int. Ed.* **2022**, *134*, e202209464.

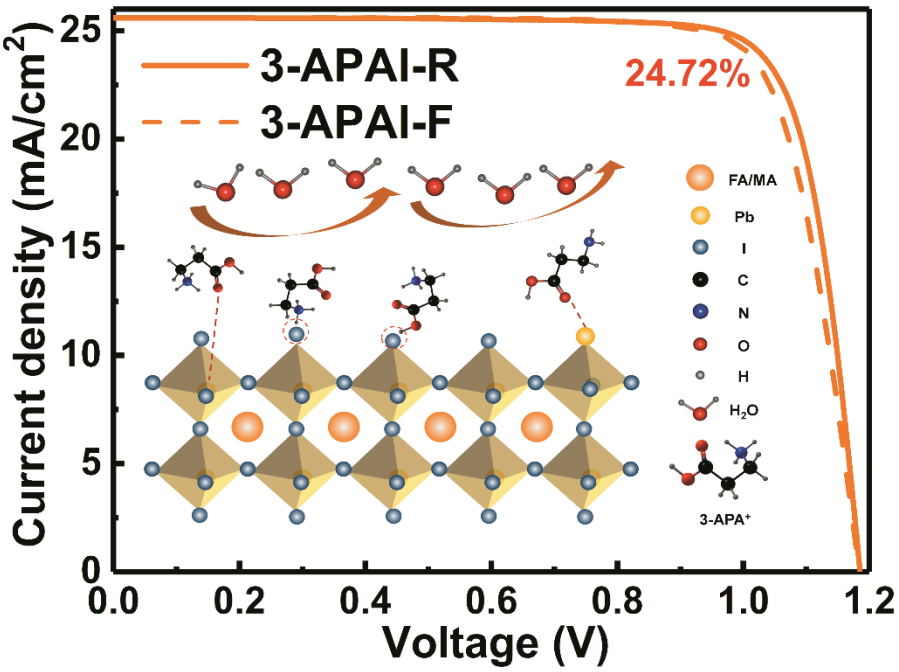

An effective interfacial defect and carrier management strategy is developed by synergistically modulating organic functional groups and spatial conformation of organic ammonium salt modification molecules. The 3-APAI modified device based on vacuum flash technology achieves an alluring peak efficiency of 24.72% (certified 23.68%), which is among highly efficient devices fabricated without antisolvents.